

Ultrafast extrinsic spin-Hall currents

E. Ya. Sherman,¹ Ali Najmaie,¹ H.M. van Driel,¹ Arthur L. Smirl,² and J.E. Sipe¹

¹*Department of Physics and Institute for Optical Sciences,
University of Toronto, 60 St. George Street,
Toronto, Ontario, Canada M5S 1A7*

²*Laboratory for Photonics and Quantum Electronics,
138 IATL, University of Iowa, Iowa City, Iowa 52242*

Abstract

We consider the possibility of ultrafast extrinsic spin-Hall currents, generated by skew scattering following the optical injection of charge or pure spin currents. We propose a phenomenological model for this effect in quantum well structures. An injected charge current leads to a spin-Hall-induced pure spin current, and an injected pure spin current leads to a spin-Hall-induced charge current. The resulting spin or charge accumulation can be measured optically.

PACS numbers: 78.20.Ls, 42.65.-k, 72.25.Fe, 73.63.Hs

I. INTRODUCTION

The spin-Hall effect (SHE), which leads to a spin current carried either by electrons or holes driven out of the equilibrium, has attracted the attention of both theorists and experimentalists because of its diverse and interesting physics, and because of possible applications in spintronics. Recent reviews of the current understanding of this effect have been presented by Engel *et al.*¹ and Schliemann². Usually two versions of the effect are distinguished. The *extrinsic* spin-Hall current is due to a spin-dependent scattering of electrons by the screened Coulomb potential of charged impurities^{3,4,5}, and arises from spin-orbit (SO) coupling corrections to the scattering potential. The *intrinsic* spin-Hall current^{1,2,6} results from electron spin precession due to SO coupling, and is understood as a band structure effect⁷. In usual scenarios for observing both effects, the electron system is initially close to the thermal equilibrium; a weak applied electric field leads to electrical currents and, through various mechanisms involving spin-orbit coupling, spin currents arise. Hence the spin current arises as a response of the system to an external static or a far-infrared electric field⁸. The fact that the system is close to equilibrium has at least two important consequences. First, the initial electron distribution is known, and the well-established techniques of response function calculations for a weakly perturbed systems can be applied. Second, the random potential of impurities, screened by the equilibrium distribution of electrons⁹, is well-known and independent of the external perturbation. At low temperatures, the charged impurities are screened on the spatial scale of the Thomas-Fermi radius in the bulk, or of the quantum well width for two-dimensional electrons.

Observations of intrinsic¹⁰ and extrinsic^{11,12} spin-Hall effects have been reported recently, with the existence and size of the effects extracted from experimentally determined spin accumulation produced by the spin current. Thus the ability to measure the spin accumulation is important for studies of the spin-Hall effect. The spin accumulation pattern is strongly sensitive to experimental conditions, and requires a thorough analysis for each experiment and sample geometry¹³.

Here we theoretically consider experiments involving the all-optical generation of a strongly nonequilibrium extrinsic spin-Hall effect in quantum wells. The approach is based on the coherent control of the interband absorption of light, which allows charge and spin current to be injected optically in bulk semiconductors and quantum wells^{14,15,16,17,18}. As a result, the system is driven strongly out of equilibrium, with the injected electrons having energies on the order of 150 meV above the bottom of the conduction band, and velocities on the order of 1000 km/s; the injected 2D electron areal concentrations n are of the order of $10^{11} - 10^{12} \text{ cm}^{-2}$. The injected charge and spin currents then relax by collision of electrons with other carriers, phonons, and impurities^{19,20} on the timescale of the order of 100 fs. Electron-hole, electron-electron, and electron-impurity collisions can lead to a spin-Hall current via the extrinsic SHE. The spin precession of photoexcited electrons due to Dresselhaus and Rashba-type SO coupling can, in general, lead to the analog of intrinsic spin current. In this paper we present a phenomenological model of the optically generated extrinsic SHE; we comment briefly on the intrinsic effect in section 6.

Because the SHE we consider is all-optically generated, it can be studied far from any

bounding surfaces of a sample, and the kind of detailed analysis of edge effects necessary in near-equilibrium experiments is not required. Further, since in principle optical excitation with a range of pulse widths can be considered, it should be possible to study the timescales involved in the SHE in a controllable way, leading to a more detailed understanding of the microscopic mechanisms responsible for it. And the far-from-equilibrium nature of the experimental scenarios we consider means that many assumptions implicitly made in the study of near-equilibrium spin-Hall effects must be reconsidered, and the subject seen in a much broader perspective.

We begin with a reminder of the experimental schemes for coherently controlled injection of current and spin current. We then consider the scattering and space charge effects that can be important in optical experiments, estimate the size of the spin-Hall effects, and finally summarize and discuss our results. While we focus on quantum well structures, many of our general conclusions will hold for experiments on bulk samples as well.

II. INJECTION SCENARIOS

Earlier we had suggested the use of spin currents generated all-optically via infrared absorption²¹ or Raman scattering^{22,23} to study spin Hall effects in doped quantum wells. Here we consider utilizing the simpler mechanisms of current or spin current injection via absorption across the band gap of an undoped quantum well. In the experiments we consider, two pulses with carrier frequencies ω and 2ω and polarizations \mathbf{e}_ω and $\mathbf{e}_{2\omega}$ are directed onto the QW, leading to an electric field

$$\mathbf{E}(t) = \mathbf{e}_\omega E_\omega(t) e^{i\phi_\omega} e^{-i\omega t} + \mathbf{e}_{2\omega} E_{2\omega}(t) e^{i\phi_{2\omega}} e^{-2i\omega t} + c.c.,$$

where $E_\omega(t)$ and $E_{2\omega}(t)$ are slowly varying amplitudes. An important parameter is the relative phase parameter $\Delta\phi = 2\phi_\omega - \phi_{2\omega}$, which is under the control of the experimentalist. The photon energy $2\hbar\omega$ is above but close to the bandgap E_g of the quantum well, and interference of one- and two-photon absorption occurs^{24,25}. We take the intensity of the incident pulses to vary in space as $\exp(-\rho^2/\Lambda^2)$, where $\rho = \sqrt{x^2 + y^2}$ is the lateral coordinate, and the spot size Λ is of the order of few microns. In the laser spot a relatively low-density electron-hole plasma is generated, with possibly a net spin depending on the polarizations chosen for the pulses¹⁵. Current and spin current can also be injected, with the injection controlled by adjusting the polarization of the two pulses^{15,24,25}. At a given (x, y) the injected areal electrical and spin current densities are given by J^i and K^{ij} respectively, where

$$J^i/n = \overline{ev^i},$$

$$K^{ij}/n = \frac{\hbar}{4} \overline{v^i \sigma^j + \sigma^j v^i},$$

with the overbar denoting an average of the indicated quantity at (x, y) , \mathbf{v} is the velocity, and $\hbar\sigma/2$ the spin; i and j are Cartesian indices. We begin by restricting ourselves to the

electrons; we return to the holes at the end of section 5. Neglecting the spin-splitting in the conduction miniband, we can write

$$\begin{aligned} J^i &= e (j_+^i + j_-^i), \\ K^{iz} &= \frac{\hbar}{2} (j_+^i - j_-^i), \end{aligned}$$

where we have introduced the (number) areal current density of spin up and spin down electrons, j_+^i and j_-^i respectively,

$$j_{\pm}^i = \int \frac{d\mathbf{k}}{(2\pi)^2} v_{cc}^i(\mathbf{k}) f_{\pm}(\mathbf{k}),$$

where $\mathbf{v}_{cc}(\mathbf{k})$ is the diagonal velocity matrix element in the conduction miniband at the two dimensional wavevector $\mathbf{k} = (k_x, k_y)$, and $f_{(+,-)}(\mathbf{k})d\mathbf{k}$ is the number of spin up (down) electrons in the corresponding element of the phase space. The resulting areal densities of spin-up and spin-down electrons are given by

$$n_{\pm} = \int \frac{d\mathbf{k}}{(2\pi)^2} f_{\pm}(\mathbf{k}),$$

and we can then define average velocities for each spin projection at a given (x, y) as

$$v_{\pm}^i = j_{\pm}^i / n_{\pm},$$

where $i = x$ or y .

In this first analysis we consider ultrafast experiments performed at or near room temperature, and a number of time scales can be identified. One is the optical pulse length, which is on the order of 100 fs. Another is that of momentum relaxation, which is typically also on the order of 100 fs. We introduce appropriate relaxation times τ_x and τ_y below, associated with motion in the indicated directions, and for the experiments we consider they can be different. But we generally expect that they are both on the order of the momentum relaxation time. Below we will derive a spin Hall scattering time τ_{sH} , defined such that the average spin-Hall force on an electron of effective mass m^* with a given spin is

$$\langle F_{\text{sH}} \rangle = m^* \langle v \rangle \tau_{\text{sH}}^{-1}, \quad (1)$$

where $\langle v \rangle$ is the average of one of the v_{\pm}^i over the indicated cloud of spins, often referred to as the "swarm" velocity, and $\langle F_{\text{sH}} \rangle$ is the corresponding average of the spin-Hall force, which will be in a direction perpendicular to $\langle v \rangle$. We will see below that $\tau_{\text{sH}} \approx 10$ ps and, since the corresponding rates satisfy $1/\tau_{\text{sH}} \gg 1/\tau_i$, the spin-Hall currents will be slaved to the momentum relaxation. We will also see that space charge effects will arise on a time scale larger than the τ_i , leading to charge oscillations that are overdamped. Finally, diffusion and recombination with holes will become important on even longer time scales. These we neglect in the treatment we present here, where our focus is on identifying the typical spin-Hall displacements that can be expected within a few hundred femtoseconds of the exciting optical pulses.

While the laser pulse is interacting with the semiconductor, spin or electrical currents, or both, can be injected, depending on the excitation geometry. Since the pulse width is comparable to the momentum relaxation time, and since the momentum relaxation time itself will change as the injected density increases during excitation, a full kinetic theory will ultimately be required to trace the distributions $f_{\pm}(\mathbf{k})$ during excitation; any other approximation during the excitation phase is inevitably a crude one. We make the simplest such approximation by separating the excitation and transport regimes, beginning our transport analysis after the spins are assumed to have been injected by the laser pulses. The velocities $\langle v_{\pm}^i \rangle$ assumed right after the injection, but before our transport analysis begins, can then be taken immediately from the kind of simple Fermi's Golden Rule calculations that have been presented in the literature^{14,15}, and at this level are independent of the density injected; since the injection pulses are on the order of 100 fs, we naturally assume that the hole spins are completely relaxed at the start of our transport analysis. Despite its simplicity, we believe that more detailed calculations will confirm the estimates this prediction provides of the early separation of the spin distributions.

We consider two excitation geometries that we label (a) and (b) (see Fig. 1). In the first (a) we take \mathbf{e}_{ω} to be oriented along the y direction and $\mathbf{e}_{2\omega}$ along the x direction; in the second (b) we take both \mathbf{e}_{ω} and $\mathbf{e}_{2\omega}$ to be oriented along the y direction. In (a) we inject a pure spin current if $\Delta\phi = 0$ (initially $\langle v_{+}^y \rangle = -\langle v_{-}^y \rangle > 0$ and $\langle v_{\pm}^x \rangle = 0$), and in (b) a pure electrical current if $\Delta\phi = \pi/2$ (initially $\langle v_{+}^y \rangle = \langle v_{-}^y \rangle < 0$ and $\langle v_{\pm}^x \rangle = 0$)²⁴; we assume these choices are made for the relative phase parameter. Then we can take the velocities $\langle v_{\pm}^i \rangle$ to vary as

$$\begin{aligned} \frac{d}{dt} \langle v_{\pm}^x \rangle &= C_{(a,b)\pm}^x(t) + S_{(a,b)\pm}^x(t), \\ \frac{d}{dt} \langle v_{\pm}^y \rangle &= C_{(a,b)\pm}^y(t) + S_{(a,b)\pm}^y(t), \end{aligned} \quad (2)$$

where the vectors $\mathbf{C}_{a\pm}(t)$ and $\mathbf{S}_{a\pm}(t)$ describe the effects of space charge and scattering in geometry (a), and with $\mathbf{C}_{b\pm}(t)$ and $\mathbf{S}_{b\pm}(t)$ the corresponding effects in geometry (b).

III. SCATTERING

We turn first to the scattering terms, which in form are independent of the excitation geometry, and can be written as

$$\begin{bmatrix} S_{\pm}^x \\ S_{\pm}^y \end{bmatrix} = \begin{bmatrix} -\tau_x^{-1} & \mp \tau_{\text{sH}}^{-1} \\ \pm \tau_{\text{sH}}^{-1} & -\tau_y^{-1} \end{bmatrix} \begin{bmatrix} \langle v_{\pm}^x \rangle \\ \langle v_{\pm}^y \rangle \end{bmatrix}. \quad (3)$$

We now confirm this form, and estimate τ_{sH} . To do this we note that the number of injected holes will be equal to the number of injected electrons, and for high excitation densities and initially clean, undoped samples we can expect the scattering of the electrons from the holes to dominate the scattering of the electrons from any impurities. We assume that the heavy holes injected can be considered approximately fixed in determining their effect on

the electrons' motion. The Hamiltonian describing the role spin-orbit coupling plays in the scattering process of electron at $\boldsymbol{\rho}$ by a hole at $\boldsymbol{\rho}_j$ then takes the form

$$H_{\text{sH}}(\boldsymbol{\rho} - \boldsymbol{\rho}_j) = \mp \frac{\hbar\gamma}{4m^*E_g} [\nabla_{\boldsymbol{\rho}}U(|\boldsymbol{\rho} - \boldsymbol{\rho}_j|), \mathbf{p}], \quad (4)$$

where the upper (lower) sign refers to a spin up (down) electron, $\gamma \equiv 2\Delta/E_g$, where Δ is the energy difference between the split-off and valence band, and the potential energy U describes Coulomb interaction between electron and hole confined in the quantum well. The total spin-orbit force acting on an electron is therefore:

$$\mathbf{F}_{\text{sH}}(\boldsymbol{\rho}) = \sum_j \mathbf{f}_{\text{sH}}(\boldsymbol{\rho} - \boldsymbol{\rho}_j), \quad (5)$$

where the force $\mathbf{f}_{\text{sH}}(\boldsymbol{\rho} - \boldsymbol{\rho}_j)$ on the electron due to hole j is given by

$$\mathbf{f}_{\text{sH}}(\boldsymbol{\rho} - \boldsymbol{\rho}_j) = -\nabla_{\boldsymbol{\rho}}H_{\text{sH}}(\boldsymbol{\rho} - \boldsymbol{\rho}_j). \quad (6)$$

The mean value of \mathbf{F}_{sH} , which we seek, is the spin- and velocity-dependent electromotive force acting on electrons. The long-range potential energy of electron-hole interaction $U(\rho)$,

$$U(\rho) = \frac{2e^2}{w\epsilon} \int_0^w \sin^2\left(\pi\frac{z_1}{w}\right) \int_0^w \sin^2\left(\pi\frac{z_2}{w}\right) \frac{dz_2dz_1}{\sqrt{\rho^2 + (z_1 - z_2)^2}},$$

where w is the width of the quantum well and ϵ the background dielectric constant, exhibits a weak logarithmic divergence at small distances

$$U(\rho) \approx \begin{cases} 3(e^2/\epsilon w) \ln(w/\rho), & \rho \ll w, \\ e^2/\epsilon\rho, & \rho \gg w. \end{cases}$$

Due to the high energy of electrons, their relatively low density, and the short times of interest here, screening effects can be assumed to be small and therefore have been neglected.

We calculate the skew scattering in a classical approximation, considering an electron with momentum $\mathbf{p} = (0, p)$ moving in the force field (5). For a spin-up electron at the origin, the x -component of the force on it due to a hole at a distance ρ in the xy plane from the electron, making an angle ζ from the x -axis (see Fig. 2) is

$$\begin{aligned} f_{\text{sH}}^x(\boldsymbol{\rho} - \boldsymbol{\rho}_h)|_{\boldsymbol{\rho}=\mathbf{0}} &= \frac{\hbar\gamma}{4m^*E_g} p \left(\frac{\partial^2 U(|\boldsymbol{\rho} - \boldsymbol{\rho}_h|)}{\partial x^2} \right)_{\boldsymbol{\rho}=\mathbf{0}} \\ &= -\frac{\hbar\gamma}{4m^*E_g} p \left(\cos^2\zeta \frac{\partial^2 U(\rho_h)}{\partial \rho_h^2} + \frac{\sin^2\zeta}{\rho_h} \frac{\partial U(\rho_h)}{\partial \rho_h} \right) \\ &\equiv g(\rho_h, \zeta, p) \end{aligned}$$

where $\boldsymbol{\rho}_h = (\rho_h \cos \zeta, \rho_h \sin \zeta)$. The mean value of this force, for holes uniformly distributed with an areal density n , is given by

$$\begin{aligned} \langle F_{\text{sH}}^x \rangle &= n \int_{0^+}^{\infty} d\rho_h \rho_h \int_{\zeta=0}^{2\pi} g(\rho_h, \zeta, p) d\zeta \\ &= -3\pi \frac{e^2 n}{\epsilon} \frac{p}{\hbar k_g} \frac{1}{k_g w}, \end{aligned} \quad (7)$$

where the integral over ρ_h is done for a small lower bound, which is then allowed to approach zero at the end of the calculation, and $k_g = 2\sqrt{E_g m^* / \gamma \hbar^2}$ is the wavevector associated with the spin-orbit coupling strength (4). Now associating p with the $m^* \langle v \rangle$ of (1), we can identify

$$\tau_{\text{sH}} = \frac{\hbar k_g^2 w \epsilon}{3\pi n e^2}, \quad (8)$$

and, repeating the calculation for a spin-down electron, confirm the signs in (3). For GaAs quantum wells we expect typical values of $k_g^2 = 2 \times 10^{15} \text{ cm}^{-2}$ and $w = 10 \text{ nm}$; for injected areal densities of $n = 10^{12} \text{ cm}^{-2}$, we find $\tau_{\text{sH}} \approx 10 \text{ ps}$. This is in comparable with a result of 20 ps found earlier²⁶ for the skew-scattering time for Coulomb drag effects, despite the different nature of the scattering potential. From (7) we see that the spin-orbit force is small in comparison to the characteristic Coulomb force ne^2/ϵ , as expected.

This treatment of the spin-Hall force is clearly a simple one; besides its mean field nature, the so-called "side-jump" component of the scattering is neglected. Our main use here of the result (8) is to help us in our estimates below of the order of the magnitude of the size of the charge and spin displacements that will result. In that respect the neglect of the side-jump component, which typically does not affect the order of magnitude of the spin-Hall scattering in the region of large momenta, should not lead to serious error^{9,27}.

To touch base with the traditional literature on the spin-Hall effect in near-equilibrium systems, we can use our phenomenological scattering description (3), with an assumed static electric field in the y direction on a sample of uniform density,

$$\frac{d}{dt} \begin{bmatrix} v_{\pm}^x \\ v_{\pm}^y \end{bmatrix} = \begin{bmatrix} -\tau^{-1} & \mp \tau_{\text{sH}}^{-1} \\ \pm \tau_{\text{sH}}^{-1} & -\tau^{-1} \end{bmatrix} \begin{bmatrix} v_{\pm}^x \\ v_{\pm}^y \end{bmatrix} + \begin{bmatrix} 0 \\ eE^y/m^* \end{bmatrix},$$

to make a steady state calculation; here, for simplicity, we have put $\tau_x = \tau_y = \tau$. We find an areal current density $J^y = \sigma E^y$, where since $\tau/\tau_{\text{sH}} \ll 1$ the conductivity $\sigma = (e^2 n \tau / m^*) (1 + \tau^2 / \tau_{\text{sH}}^2)^{-1}$ is only slightly modified from the usual result $e^2 n \tau / m^*$, and an areal spin current density $K^{xz} = \sigma_{\text{sH}} E^y$, where

$$\sigma_{\text{sH}} = \frac{\hbar}{2|e|} \frac{\tau}{\tau_{\text{sH}}} \sigma. \quad (9)$$

The ratio $\tau/\tau_{\text{sH}} \approx 0.01$ we find here is considerably less than predicted for 2DEG systems²⁶, because the relaxation time τ is much longer in those samples. But our result is comparable to the spin-Hall angle τ/τ_{sH} predicted for doped quantum wells with impurities in the well⁹, a situation roughly comparable to ours, but with impurities playing the role of the holes.

IV. SPACE CHARGE EFFECTS

In the experimental geometries we consider, space charge effects arise as the holes and electrons separate; their strength can be characterized by the plasma frequency. Consider first a simple example where the center of charge of an electron distribution is displaced a distance x from the center of charge of the corresponding hole distribution, assumed

fixed. Neglecting any diffusion of the charges and considering only ballistic motion, familiar elementary arguments give that the velocity v of the center of the electron charge distribution satisfies the equation

$$\frac{dv}{dt} = -\Omega^2 x,$$

where Ω is the plasma frequency for the given charge pattern. For a rigid Gaussian distribution of electrons and holes of the form $n \exp(-\rho^2/\Lambda^2)$ in a single quantum well²⁸, the effective plasma frequency is given by

$$\Omega^2 = \left(\frac{\pi}{2}\right)^{3/2} \frac{ne^2}{\epsilon m^* \Lambda}. \quad (10)$$

This dependence of the plasma frequency on Λ is characteristic of 2D plasma oscillations, and does not arise for plasma oscillation in three dimensions; in the geometries we consider here we can take Λ to be of the order of the laser spot size injecting the carriers. For characteristic GaAs parameters, an assumed injected areal carrier density of $n = 10^{12} \text{ cm}^{-2}$, and $\Lambda = 2 \mu\text{m}$, we find $\Omega^2 \tau^2 \approx 0.03$, where we have taken a momentum relaxation time of $\tau = 100 \text{ fs}$. In a multiple quantum well (MQW) structure consisting of N_{QW} identical quantum wells each with areal density n , and far from any dielectric/air interface, the plasma frequency is approximately given by $\Omega^2 = N_{\text{QW}}(\pi/2)^{3/2} ne^2 / (\epsilon m^* \Lambda)$, if the total thickness of the structure is much less than Λ ; this condition is well-satisfied for widely used structures with $N_{\text{QW}} \lesssim 10$ and the sum of the well and barrier thicknesses $\lesssim 30 \text{ nm}$. If all the quantum wells are much closer than Λ to a dielectric/air interface, Ω^2 will be enhanced by a factor of $2\epsilon/(\epsilon+1)$. Even for such structures we have $\Omega^2 \tau^2 < 1$, and momentum relaxation will control the evolution of carrier velocities initially, space charge effects arising only after the injected velocities have considerably slowed. Nonetheless, since Ω^{-1} is much shorter than typical diffusion times, we can estimate the consequences of space charge effects by neglecting any change in the distribution of electrons other than the motion of their center of charge $\langle \boldsymbol{\rho}_{\pm} \rangle = (\langle x_{\pm} \rangle, \langle y_{\pm} \rangle)$, where $\langle x_{+} \rangle$ is the x -component of the center of charge of spin-up electrons, etc.

Charge separation occurs in characteristically different ways in our two geometries (see Fig. 1). In geometry (a) the two electron distributions (spin-up and spin-down) initially separate from a hole distribution remaining, in our neglect of hole velocities, centered at the origin. A "quadrupole-type" charge separation in the y direction results, and space charge effects will here be small. The charge separation of spin-up and spin-down carriers in the x direction will be the same direction, however, and there will be none of the cancellation that occurs in the y direction. Hence, to first approximation, in geometry (a) we can write

$$\begin{bmatrix} C_{a\pm}^x \\ C_{a\pm}^y \end{bmatrix} = \begin{bmatrix} -\Omega_x^2 & 0 \\ 0 & 0 \end{bmatrix} \begin{bmatrix} \langle x_{\pm} \rangle \\ \langle y_{\pm} \rangle \end{bmatrix}, \quad (11)$$

where we will take Ω_x (and Ω_y below) to be given by (10) or its generalization to multiple quantum wells, but use the subscript to indicate the geometry. In geometry (b) the situation is reversed; there are significant space charge effects only in the y direction, and we have

$$\begin{bmatrix} C_{b\pm}^x \\ C_{b\pm}^y \end{bmatrix} = \begin{bmatrix} 0 & 0 \\ 0 & -\Omega_y^2 \end{bmatrix} \begin{bmatrix} \langle x_{\pm} \rangle \\ \langle y_{\pm} \rangle \end{bmatrix}. \quad (12)$$

V. CHARGE AND SPIN DYNAMICS

We can now assemble and solve our approximate dynamical equations for the two geometries we have considered. We begin with geometry (a). Here the injection yields $\langle v_{\pm}^y(0) \rangle \equiv \pm v_0$, where v_0 is the initial speed of the injected spins, and $\langle v_{\pm}^x(0) \rangle = 0$. Combining the scattering (3) and space charge (11) effects in our dynamical equations (2), we find

$$\frac{d}{dt} \begin{bmatrix} \langle v_{\pm}^x \rangle \\ \langle v_{\pm}^y \rangle \end{bmatrix} = \begin{bmatrix} -\tau_x^{-1} & \mp \tau_{\text{sH}}^{-1} \\ \pm \tau_{\text{sH}}^{-1} & -\tau_y^{-1} \end{bmatrix} \begin{bmatrix} \langle v_{\pm}^x \rangle \\ \langle v_{\pm}^y \rangle \end{bmatrix} + \begin{bmatrix} -\Omega_x^2 & 0 \\ 0 & 0 \end{bmatrix} \begin{bmatrix} \langle x_{\pm} \rangle \\ \langle y_{\pm} \rangle \end{bmatrix}. \quad (13)$$

In solving for $\langle v_{\pm}^y \rangle$ we can justifiably neglect the back-effect due to the spin-Hall scattering from the small $\langle v_{\pm}^x \rangle$, which is itself generated from spin-Hall scattering. We find

$$\langle v_{\pm}^y \rangle = \pm v_0 e^{-t/\tau_y},$$

and using this in (13) we can solve for $\langle v_{\pm}^x \rangle$, together $\langle y_{\pm} \rangle$ and $\langle x_{\pm} \rangle$, using $d \langle y_{\pm} \rangle / dt = \langle v_{\pm}^y \rangle$ and $d \langle x_{\pm} \rangle / dt = \langle v_{\pm}^x \rangle$. The results are

$$\langle y_{\pm} \rangle = \pm v_0 \tau_y (1 - e^{-t/\tau_y})$$

and

$$\begin{aligned} \langle x_{\pm} \rangle &= \mp a_{\text{PSC}} \left\{ e^{-t/\tau_y} + \left(\frac{\tau_x^-}{\tau_x^+ - \tau_x^-} \left(\frac{\tau_x^+}{\tau_y} - 1 \right) - 1 \right) e^{-t/\tau_x^+} \right. \\ &\quad \left. + \frac{\tau_x^-}{\tau_x^+ - \tau_x^-} \left(1 - \frac{\tau_x^+}{\tau_y} \right) e^{-t/\tau_x^-} \right\}, \end{aligned}$$

where

$$a_{\text{PSC}} = \frac{v_0}{\tau_{\text{sH}}} \frac{\tau_y^2 \tau_x}{\tau_x - \tau_y + \Omega_x^2 \tau_y^2 \tau_x},$$

and

$$\frac{1}{\tau_x^{\pm}} \equiv \frac{1}{2} \left(\frac{1}{\tau_x} \pm \sqrt{\frac{1}{\tau_x^2} - 4\Omega_x^2} \right); \quad (14)$$

note that $\tau_x^+ \approx \tau_x^{-1}$ and sets a short time scale for the evolution of $\langle x_{\pm} \rangle$, and $\tau_x^- \approx (\Omega_x^2 \tau_x)^{-1}$, which sets a longer time scale. The results for $\langle y \rangle \equiv |\langle y_{\pm} \rangle|$ and $\langle x \rangle \equiv |\langle x_{\pm} \rangle|$ are given in Fig. 3a. We have assumed that electrons are injected about 150 meV above the bottom of the conduction band, leading to an injected swarm velocity of $v_0 = 500$ km/s for the electrons. In choosing the other parameters we have in mind a typical momentum relaxation time $\tau = 100$ fs. Thus we set $\tau_x = 100$ fs but take $\tau_y = 50$ fs, shorter than the momentum relaxation time, because the spin current can be expected to relax on a faster time scale than current, there being many scattering mechanisms that can redistribute spin without redistributing momentum^{19,20}; in line with the discussion in section 4 above and using Eq.(10) to evaluate the plasma frequency, we take $\Omega_x \tau = 0.15$ (weak space charge effects, solid lines) for a single quantum well and $\Omega_x \tau = 0.4$ (considerable space charge effects, dashed lines) for the

$N_{\text{QW}} = 8$ structure, with the wells far from a dielectric/air interface. As a result of space charge effect, $\langle x \rangle$ decreases back to zero at the time scale dependent on $\Omega_x \tau$ as the dipole charge separation pulls the electrons back to the holes. Since we have neglected the weaker, quadrupole type space charge effects that arise in the y direction, even here $\langle y \rangle$ does not relax at long times. A more realistic calculation of space charge effects would of course show a decrease in $\langle y \rangle$, but on a longer time scale than that exhibited by the decay of $\langle x \rangle$ in Fig. 3a.

For geometry (b) our dynamical equations are

$$\frac{d}{dt} \begin{bmatrix} \langle v_{\pm}^x \rangle \\ \langle v_{\pm}^y \rangle \end{bmatrix} = \begin{bmatrix} -\tau_x^{-1} & \mp \tau_{\text{sH}}^{-1} \\ \pm \tau_{\text{sH}}^{-1} & -\tau_y^{-1} \end{bmatrix} \begin{bmatrix} \langle v_{\pm}^x \rangle \\ \langle v_{\pm}^y \rangle \end{bmatrix} + \begin{bmatrix} 0 & 0 \\ 0 & -\Omega_y^2 \end{bmatrix} \begin{bmatrix} \langle x_{\pm} \rangle \\ \langle y_{\pm} \rangle \end{bmatrix}, \quad (15)$$

and space charge effects enter immediately in the evolution of $\langle v_{\pm}^y \rangle$, since we are injecting a net current with $\langle v_{\pm}^y(0) \rangle \equiv -v_0$. Again we have $\langle v_{\pm}^x(0) \rangle = 0$, so we neglect the small spin-Hall contribution of the generated $\langle v_{\pm}^x \rangle$ on $\langle v_{\pm}^y \rangle$ and, solving the second of (15) together with $d\langle y_{\pm} \rangle/dt = \langle v_{\pm}^y \rangle$ yields

$$\langle v_{\pm}^y \rangle = \frac{-v_0}{\sqrt{\tau_y^{-2} - 4\Omega_y^2}} \left\{ \frac{1}{\tau_y^+} \exp[-t/\tau_y^+] - \frac{1}{\tau_y^-} \exp[-t/\tau_y^-] \right\},$$

and

$$\langle y_{\pm} \rangle = \frac{-v_0}{\sqrt{\tau_y^{-2} - 4\Omega_y^2}} \left\{ (1 - \exp[-t/\tau_y^+]) - (1 - \exp[-t/\tau_y^-]) \right\}$$

where τ_y^{\pm} are defined in terms of τ_y and Ω_y as are τ_x^{\pm} in terms of τ_x and Ω_x (14). The minus sign in front of v_0 here is due to the fact that at $2\phi_{\omega} - \phi_{2\omega} = \pi/2$, which maximizes the injected current, the electrons move in the $-y$ -direction, as shown in Fig.1(b). A straightforward integration of the second of (15) and $d\langle x_{\pm} \rangle/dt = \langle v_{\pm}^x \rangle$ then yields

$$\begin{aligned} & \langle x_{\pm} \rangle \\ &= \mp a_C \left\{ \frac{\tau_y^+}{\tau_x - \tau_y^+} e^{-\tau/\tau_y^+} - \left(\frac{\tau_y^+}{\tau_x - \tau_y^+} - \frac{\tau_y^-}{\tau_x - \tau_y^-} \right) e^{-t/\tau_x} - \frac{\tau_y^-}{\tau_x - \tau_y^-} e^{-t/\tau_y^-} \right\}, \end{aligned}$$

where

$$a_C = \frac{-v_0}{\tau_{\text{sH}}} \frac{\tau_x}{\sqrt{\tau_y^{-2} - 4\Omega_y^2}}.$$

The results for $\langle y \rangle \equiv |\langle y_{\pm} \rangle|$ and $\langle x \rangle \equiv |\langle x_{\pm} \rangle|$ are plotted in Fig. Here we take $\tau_x = 50$ fs and $\tau_y = 100$ fs, since in this geometry the form corresponds to the relaxation of spin current and the latter the relaxation of current; all other parameter values are as used above. In this excitation geometry the space charge effects impact the evolution of $\langle x \rangle$ indirectly within our model, through their effects on $\langle v_{\pm}^y \rangle$ as the electrons pull away from the holes in the y direction; the resulting decrease in $\langle v_{\pm}^y \rangle$ leads to less spin-Hall current than would otherwise be induced. Since here the separation of $\langle x_{\pm} \rangle$ leads to a quadrupole type space charge effect that we neglect, there is no direct space charge effect on $\langle x \rangle$ in our model.

Despite the differences in the way space charge effects modify the dynamics in these two geometries, the inequalities $\Omega_{x,y}^2 \tau_{x,y}^2 \ll 1$ guarantee that these effects enter on a longer

time scale than the current and spin current relaxation times (τ_y and τ_x respectively in our scenarios), and thus the maximum values of $\langle y \rangle$ and $\langle x \rangle$ can be estimated neglecting space charge effects; these estimates are

$$\begin{aligned}\langle y \rangle_{\max} &= v_0 \tau_y, \\ \langle x \rangle_{\max} &= v_0 \tau_y \frac{\tau_x}{\tau_{\text{sH}}}\end{aligned}\tag{16}$$

Comparing the dashed and solid lines in Figs. 2a,b shows that within our model these estimates are valid to within about 20%, and somewhat better than that for the ratio $\langle x \rangle_{\max} / \langle y \rangle_{\max}$. Note that this ratio will be different in geometry (a) than in geometry (b), because in the former τ_x identifies the current relaxation time, and in the latter the spin current relaxation time. However, these times should be the same within a factor of two^{19,20}, which is what we have assumed above. For the parameters we have adopted here, in geometry (a) we find $\langle y \rangle_{\max} = 25$ nm and $\langle x \rangle_{\max} = 0.25$ nm; in geometry (b) we find $\langle y \rangle_{\max} = 50$ nm and $\langle x \rangle_{\max} = 0.25$ nm.

We conclude this section by returning to the holes, the motion of which we have neglected in our analysis. In the approximation of parabolic bands, the injected momentum of the holes will be equal in magnitude to the injected momentum of the electrons, and in the opposite direction. Even if we move beyond this approximation, we can generally expect the swarm velocity of the holes to be much less than that of the electrons, due to their larger effective mass. Therefore, the holes will move considerably less than the electrons, and their motion will not qualitatively affect our results. This is because what is crucial to our dynamical equations is the separation of the electrons from the holes. And to first approximation that can be described by the equations used here, with at most a modification of the electron effective mass to describe the motion of the relative electron-hole separation. For longer time scales, of course, a more detailed dynamical treatment of the electron-hole plasma would be necessary.

VI. SUMMARY AND DISCUSSION

We have presented a simple theoretical description of what might be called an "ultrafast spin-Hall effect," or rather a family of such effects. In one scenario a spin current is optically injected in the sample, and the spin-Hall effect leads to an electrical current; in the other scenario an electrical current is optically injected in the sample, and the spin-Hall effect leads to a pure spin current. Although our analysis has focused on updoped quantum wells, it should hold qualitatively for intrinsic bulk samples as well, with appropriate values for plasma frequency and relaxation times. And while we have focused on optical injection via an interference between one- and two-photon absorption across the band gap^{14,15,24,25}, other injection scenarios involving the absorption of a single laser pulse^{21,29,30}, or Raman scattering in the infrared²² or visible²³ should also lead to such ultrafast spin-Hall effects; we plan to turn to these in later communications. The ultrafast nature of these effects arises because the currents (or spin currents) can be injected on the timescale of 100 fs, and the resulting spin currents (or currents) that result from the spin-Hall effect are slaved to the injection

and relaxation of these injected currents, which also occurs on a timescale of 100 fs. Thus they should be distinguished from other effects that follow optical injection but occur on a longer time scale, such as the proposal of Bakun *et al.*³¹, where the spin current arises due a relatively slow ambipolar diffusion of injected spin-polarized electrons with their spins precessing in an applied magnetic field.

The treatment we have presented here is very elementary, most importantly in that we have artificially separated the injection and relaxation processes. In practice these occur simultaneously, and a full kinetic treatment will be essential to give a correct description of the injection and relaxation processes; such a calculation is underway. Our treatment of space charge effects is also a very simple one. But for the subpicosecond time scales of interest, and typical spot sizes, we have argued that for a single quantum well, or a MQW sample with a few wells, the main consequence of space charge effects will be to relax the maximum spin and charge displacements that are generated. Those maximum displacements can be reasonably estimated neglecting space charge effects. Indeed, in quantum well geometries the space charge effects can be reduced to some extent by using a larger spot size than is usual, and hence decreasing Ω (10). In the geometry (a) we considered, the charge displacement $\langle x \rangle_{\max}$ could be observed by the change in light transmission through the quantum wells, while in geometry (b) the spin displacement $\langle x \rangle_{\max}$ could be observed by monitoring the absorption of a circularly polarized probe pulse. The distances involved are on the order of those observed in other experiments³⁰, and so experimental study of these ultrafast effects should be feasible. Preliminary observations of these effects have already been reported³², however in experiments that have not time-resolved the motion of the carriers.

The moniker "ultrafast spin-Hall effects" is truly justified for these phenomena because the ratio of the skew-scattering-induced effect (whether it be current or spin current) to the directly injected effect (spin current or current, respectively), is given by

$$\frac{\langle x \rangle_{\max}}{\langle y \rangle_{\max}} = \frac{\tau_x}{\tau_{\text{sH}}}$$

(see (16)) which, except for the subtlety mentioned after (16), is essentially the same factor determining the ratio of the spin Hall conductivity to the conductivity, $\sigma_{\text{sH}}/\sigma$ (see (9)). Hence a measurement of $\langle x \rangle_{\max} / \langle y \rangle_{\max}$ in these ultrafast experiments is essentially a direct analog of the measurement of the spin-Hall voltage in more usual, near-equilibrium transport experiments.

Of course, this simple analogy can break down in MQW experiments using samples with a large number of wells. The significance of space charge effects is characterized by the product $\Omega^2\tau^2$, which is proportional to the number of quantum wells in a sample. As we consider increasing $\Omega^2\tau^2$, the first effect is a small, benign decrease in the maximum currents and spin currents, as shown in Fig. 3. But as $\Omega^2\tau^2$ approaches unity, a clear separation between the fast increase and slow relaxation times for the currents becomes impossible, and the overdamped motion of the electron cloud is replaced by damped oscillations. Since in practice this will happen as $\Omega^2\tau_p^2$ also approaches unity, where τ_p is the duration of the excitation pulses, in this regime injection, scattering, and space charge effects will all have to be considered together in a quantum kinetic description. We also mention that both

τ and τ_{SH} will be modified as we move to samples with larger numbers of quantum wells, since electrons in one well will interact to some extent with holes in all wells. Hence, just as Ω is modified by moving to samples of larger numbers of quantum wells, τ and τ_{SH} will be modified as well.

But while added complexity can arise due to space charge effects in MQW samples, qualitatively new physics will appear as well. Plasma frequencies are eigenfrequencies for charge oscillation, and in a structure with N_{QW} quantum wells there will be N_{QW} such frequencies, with the single frequency Ω we have identified corresponding to identical oscillation in all wells. If the relative phase parameter $\Delta\phi = 2\phi_{\omega} - \phi_{2\omega}$ is constant as the optical pulses propagate into a sample, only this mode will be excited. However, due to different refractive indices of the sample at ω and 2ω , in fact $\Delta\phi$ will vary from one well to another, and a number of plasma eigenmodes will actually be excited. The interesting physics here is clearly beyond the scope of the present paper.

We also defer to a later communication a discussion of the ultrafast analog of the intrinsic spin-Hall effect. While we have only treated the extrinsic Hall effect here, in a (001) GaAs quantum well we can expect an intrinsic effect if both the Dresselhaus³³ and Rashba³⁴ SO couplings are present, in which case the spin precession rate depends on the direction of the electron momentum. In such a sample, at typical values of the Rashba and Dresselhaus couplings the intrinsic-like and extrinsic spin Hall effects on the photoexcited electrons can be comparable. However, in symmetric quantum wells the analog of the intrinsic spin Hall effect is absent and, therefore, the kind of experiments we have discussed here will be sensitive to the extrinsic spin-Hall current.

Such experiments and their description will extend spin-Hall physics beyond the usual near-equilibrium regime in which it has been studied to date. One advantage of the optical experiments we have proposed is that laser spots can be directed away from any surfaces or edges of a sample, and thus the treatment of these regions that complicates the analysis of more usual transport experiments is not present. Another is that, by choosing the laser photon energy and hence the energy of the injected carriers, the scattering processes involved can be studied as a function of energy. But perhaps the main advantage is that ultrafast experiments allow for the study and isolation of different time scales in the problem. The analysis of this communication, for example, clearly fails for timescales longer than about a picosecond, when more complicated space charge dynamics, diffusion, and recombination effects become important. And indeed even optical experiments which probe the sample on such longer time scales will require a more detailed analysis than we present here. But effects on such longer timescales are irrelevant for the subpicosecond time scale that characterize the scattering and skew-scattering that are of primary interest. And so we believe it will be time-resolved experiments on the subpicosecond scale, for which the analysis in this communication provides a starting point, that will make the most important contribution to our understanding of the fundamental processes of interest in spintronics.

Acknowledgement This research was supported by the NSERC and DARPA SpinS program. We are grateful to I. Rumyantsev and E. Hankiewicz for very valuable discussions.

-
- ¹ H.-A. Engel, E. I. Rashba, and B. I. Halperin, preprint cond-mat/0603306
- ² J. Schliemann, preprint cond-mat/0602330
- ³ M.I. Dyakonov and V.I. Perel', Phys. Lett. A **35**, 459 (1971).
- ⁴ V.N. Abakumov and I.N. Yassievich, Sov. Phys. JETPh **34**, 1375 (1972). [Zh. Exp. Theor. Phys. **61**, 2571 (1972)], P. Nozieres and C. Lewiner, Journal de Physique, **10**, 901 (1973).
- ⁵ J. Hirsch, Phys. Rev. Lett. **83**, 1834 (1999).
- ⁶ J. Sinova, D. Culcer, Q. Niu, N. A. Sinitsyn, T. Jungwirth, and A. H. MacDonald, Phys. Rev. Lett. **92**, 126603 (2004).
- ⁷ S. Murakami, N. Nagaosa, and S.-C. Zhang, Science **301**, 1348 (2003).
- ⁸ E. I. Rashba, Phys. Rev. B **70**, 161201 (2004)
- ⁹ H. C. Huang, O. Voskoboynikov, and C. P. Lee, J. Appl. Phys. **95**, 1918 (2004).
- ¹⁰ J. Wunderlich, B. Kaestner, J. Sinova, and T. Jungwirth, Phys. Rev. Lett. **94**, 047204 (2005)
- ¹¹ Y. K. Kato, R. C. Myers, A. C. Gossard, and D. D. Awschalom, Science **306**, 1910 (2004)
- ¹² V. Sih, R. C. Myers, Y. K. Kato, W. H. Lau, A. C. Gossard, D. D. Awschalom, Nature Physics **1**, 31 (2005).
- ¹³ E. G. Mishchenko, A. V. Shytov, and B. I. Halperin, Phys. Rev. Lett. **93**, 226602 (2004)
- ¹⁴ R. D. R. Bhat and J. E. Sipe, Phys. Rev. Lett. **85**, 5432 (2000).
- ¹⁵ Ali Najmaie, R.D.R. Bhat, and J. E. Sipe, Phys. Rev. B **68**, 165348 (2003)
- ¹⁶ M. J. Stevens, A. Najmaie, R. D. R. Bhat, J. E. Sipe, and H. M. van Driel, and A.L. Smirl, J. Appl. Phys. **94**, 4999 (2003).
- ¹⁷ J. Hübner, W.W. Rühle, M. Klude, D. Hommel, R.D.R. Bhat, J.E. Sipe, and H.M van Driel, Phys. Rev. Lett. **90**, 216601 (2003).
- ¹⁸ M. J. Stevens, A. L. Smirl, R. D. R. Bhat, A. Najmaie, J. E. Sipe, and H. M. van Driel, Phys. Rev. Lett. **90**, 136603 (2003).
- ¹⁹ I. Rumyantsev, A. Najmaie, R. D. R. Bhat, and J. E. Sipe, in International Quantum Electronics Conference 2004 (IEEE, Piscataway, NJ, 2004) p.486.
- ²⁰ H. T. Duc, T. Meier, and S. W. Koch, Phys. Rev. Lett. **95**, 086606 (2005)
- ²¹ E. Ya. Sherman, Ali Najmaie, and J. E. Sipe, Appl. Phys. Lett. **86**, 122103 (2005)
- ²² Ali Najmaie, E. Ya. Sherman, and J. E. Sipe, Phys. Rev. Lett. **95**, 056601 (2005)
- ²³ Ali Najmaie, E. Ya. Sherman, and J. E. Sipe Phys. Rev. B **72**, 041304 (2005)
- ²⁴ H. M. van Driel and J. E. Sipe, in "Ultrafast phenomena in semiconductors" Chap. 5 (K-T. Tsens, Ed., Springer, 2001)
- ²⁵ M. J. Stevens, R.D.R. Bhat, Ali Najmaie, H.M. van Driel, J.E. Sipe, and A.L. Smirl, in "Optics of semiconductors and their nanostructures", p. 209 (H. Kalt and M. Hetterich, Eds., Springer, 2004)
- ²⁶ E. M. Hankiewicz and G. Vignale, Phys. Rev. B **73**, 115339 (2006)
- ²⁷ H.-A. Engel, B.I. Halperin, and E.I. Rashba, Phys. Rev. Lett. **95**, 166605 (2005)
- ²⁸ T. Ando, A. B. Fowler and F. Stern, Rev. Mod. Phys. **54**, 437 (1982).
- ²⁹ R. D. R Bhat, F. Nastos, Ali Najmaie, and J. E. Sipe, Phys. Rev. Lett. **94**, 096603 (2005)

- ³⁰ H. Zhao, X. Pan, A. L. Smirl, R. D. R. Bhat, Ali Najmaie, J. E. Sipe, and H. M. van Driel, Phys. Rev. B **72**, 201302 (2005)
- ³¹ A.A. Bakun, B.P. Zakharchenya, A.A. Rogachev, M.N. Tkachuk, and V.G. Fleisher, JETP Lett. **40**, 1293 (1984) [Pis'ma Zh. Exp. Theor. Phys. **11**, 464 (1984).]
- ³² Hui Zhao, Eric J. Loren, H. M. van Driel, and Arthur L. Smirl, Phys. Rev. Lett. **96**, 246601 (2006)
- ³³ M.I. Dyakonov and Y.Yu. Kachorovskii, Sov. Phys. Semicond. **20**, 110 (1986). For holes, see: E.I. Rashba and E.Ya. Sherman, Phys. Lett. **A 129**, 175 (1988).
- ³⁴ Yu. A. Bychkov and E. I. Rashba, JETP Lett. **39**, 79 (1984), E.I. Rashba, Sov. Phys. - Solid State **2**, 1874, (1964).

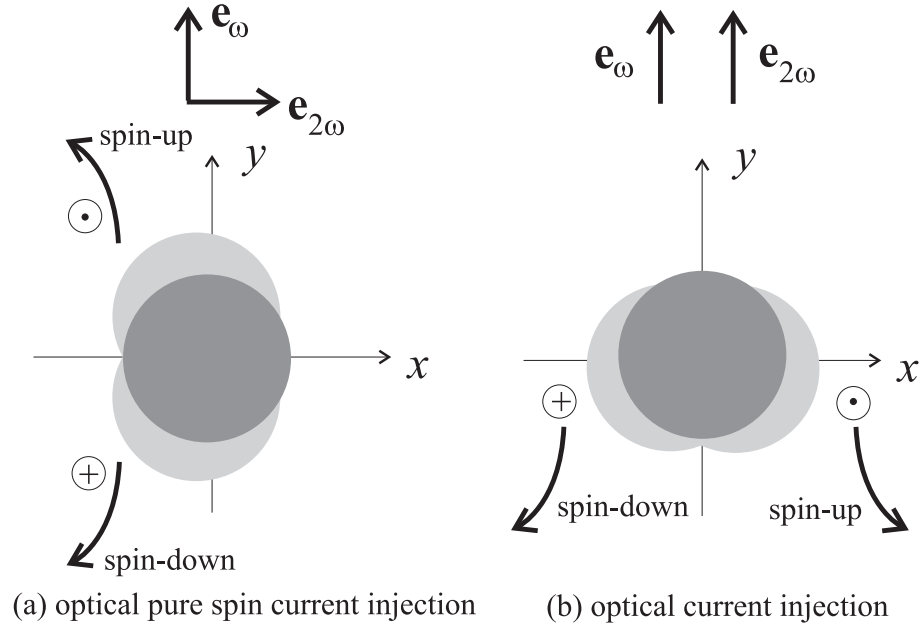


FIG. 1: The pure spin current (a) and charge current (b) injection schemes for studying the ultrafast spin-Hall effect. The curved arrows show the directions of motion of electrons with a given spin projection due to the spin-Hall effect. Dark-grey spots show holes and light-grey spots correspond to the electrons.

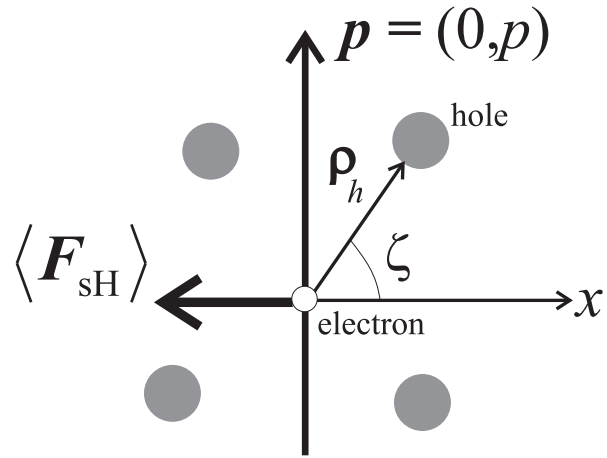


FIG. 2: The sketch of an electron with momentum $\mathbf{p} = (0, p)$ interacting with a background of holes.

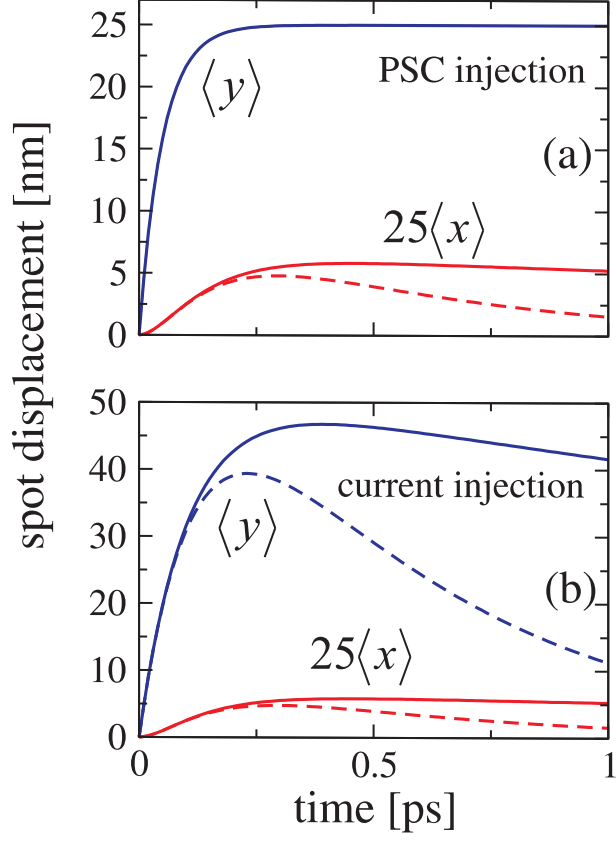


FIG. 3: The displacements of spots in the pure spin-current (PSC) (a) and charge current (b) injection schemes. We adopt (see text) a momentum relaxation time of $\tau = 100$ fs, a spin current relaxation time of 50 fs, a spin Hall time $\tau_{\text{sH}} = 10$ ps, and plasma frequencies are given by $\Omega\tau = 0.15$ (solid lines) and $\Omega\tau = 0.4$ (dashed lines). The initial swarm velocity is 500 km/s. Note that the PSC displacement ($\langle y \rangle$ in Fig. 3a) does not depend on space charge effects in our model.